Chapter-4

Electrochemical behaviour of lead-free Sn-0.7Cu-xIn solders alloys in 3.5 wt. % NaCl solution

4.1 Introduction

The alloying process is an efficient way to obtain the refined microstructure of solders; Sn-0.7Cu alloy, for instance, has been found that the fine microstructure was achieved after alloying with Ni, Ag, and Al, and there was an increase in the oxidation resistance[133][134]. The addition of In will enhance the mechanical properties and wettability of Sn-0.7Cu[135].

Indium (In) is a valuable component for solving the high melting point and low wettability of solder alloy on Cu substrate[136][137]. The main advantages of adding indium have a significant effect on the corrosion resistance corrosion of solder alloy Sn-0.7Cu. The addition of In the solder alloys of Sn-0.7Cu-xIn in improving corrosion resistance by forming a better passivation film during polarisation in 3.5 wt% NaCl, protect the surface against further corrosion [138][78][121][139]. Other researchers report many advantages to adding indium in lead-free solder alloys. Decreases the melting temperature and increases the melting range, solder corrosion rate, and hardness decrease, and lead-free solder wettability is improved [140]. The thickness ratio of IMC Cu_3Sn/Cu_6Sn_5 is lowered, and Improved solder alloy corrosion resistance and shear strength [141] [142].

In this article, an attempt has been made to synthesize Cu-Sn-In alloys with different compositions of indium in this alloy, keeping the composition of the Cu and Sn constant by vacuum induction technique. Then the composition and morphology of the alloys were investigated by metallographic methods. Then the corrosion measurements were carried out to see the effect of indium on the corrosion resistance of the alloys by potentiodynamic polarization (PD) test and wet loss method. Then the samples were subjected to SEM and XRD analysis to analyze the composition of the corrosion product.

The corrosion mechanism was then predicted by combining the potentiodynamic polarization test and Electrochemical Impedance Spectroscopy (EIS).

4.2 Results and discussion

4.2 Microstructure Characterization

The optical microstructure analysis of lead-free solder alloys Sn-0.7Cu-xIn (x=0, 0.1, 0.2, and 0.3 wt.%) is shown in Fig. 4.1. It showed two different contrasts: the dark region, which seems to be precipitation during the solidification of Cu_6Sn_5 (IMC), and the light phase of the β-Sn phase matrix (4.1.d). Nucleation of binary Sn-0.7Cu liquid alloy takes place at approximately 227^0C (eutectic temperature). Liquid Sn-0.7Cu transfers to β-Sn and Cu_6Sn_5 ($L \rightarrow Cu_6Sn_5/Cu_3Sn$ + β-Sn), consistent with Sn-0.7Cu binary phase diagram. The main principal additives of the Sn–0.7Cu solidified alloys are Cu_6Sn_5 and β-Sn. At eutectic temperature (227^0C), the dissolution of the Cu_6Sn_5 is triggered, and the Cu_6Sn_5 eutectic is grown through β-Sn diffusion. A small volume of Cu_2In phase precipitated was seen in Sn-0.7Cu-xIn solder alloy due to indium's addition from 1 to 3 wt% in the Sn-0.7Cu solder alloy. The uniform microstructure of Sn-Cu-In solder alloys has been obtained with the addition of the Indium element, and β-Sn grains have significantly been refined. The microstructure of refined solder alloys contributed to a more uniform phase distribution, which benefited the superior mechanical properties [143].

The experiment was carried out with XRD, and corresponding results are shown in Fig. 4.2. One can see that Sn-0.7Cu, Sn-0.7Cu-1In, Sn-0.7Cu-2In, and Sn-0.7Cu-3In consist of the pattern of β-Sn, Sn_3Cu, Sn_6Cu_5, and Cu_2In, while a pattern of variation of Indium in Sn-0.7Cu includes some Cu_2In peaks with 2 theta scales between 43 to 45 degrees.

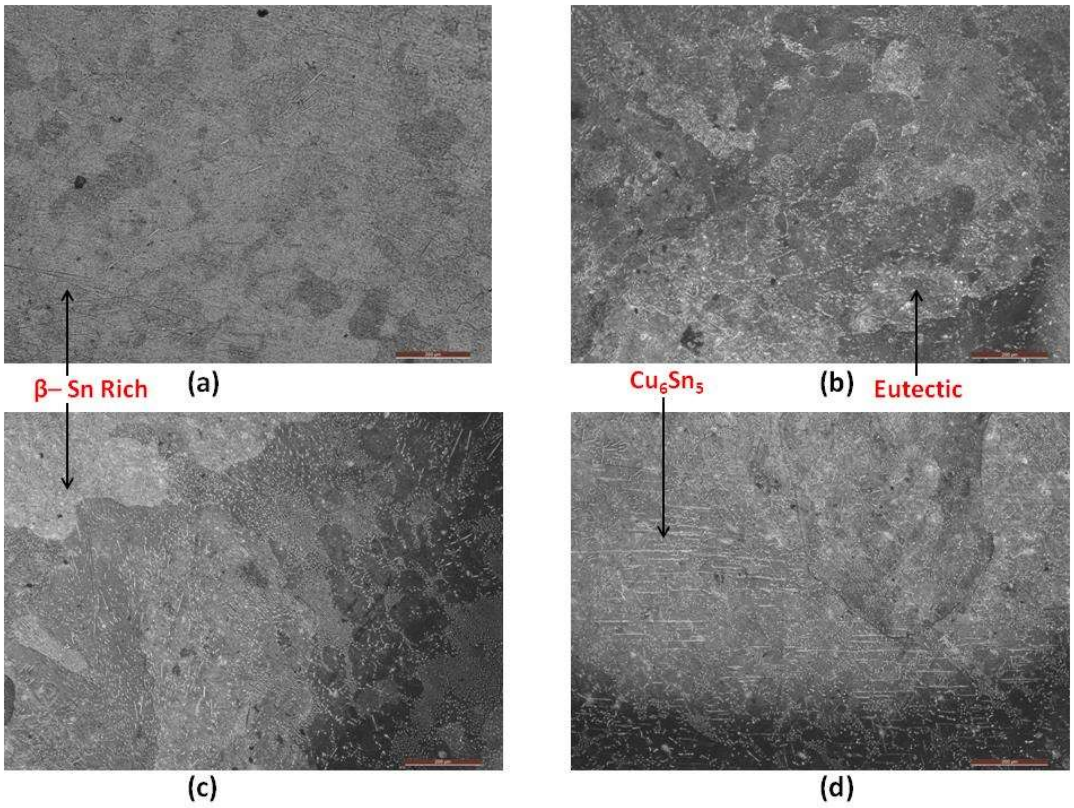

Fig.4. 1 Optical microstructures of solder alloys (a) Sn–0.7Cu, (b) Sn–0.7Cu–1In, (c) Sn–0.7Cu–2In, and (d) Sn–0.7Cu–3In.

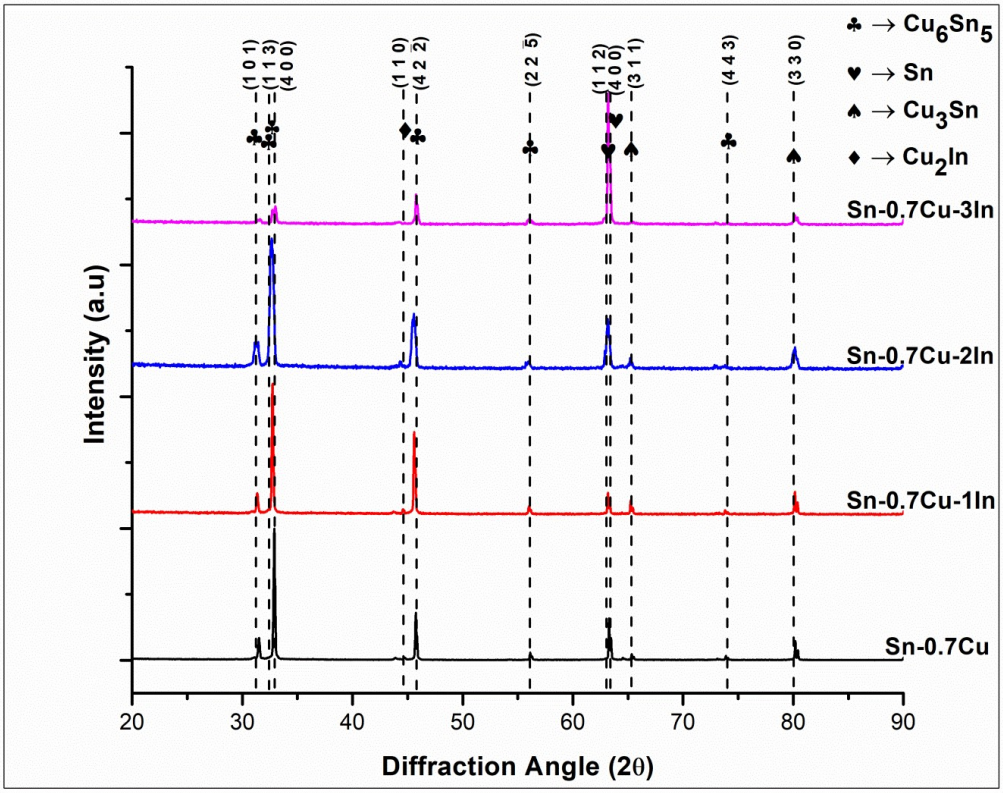

Fig.4. 2 XRD pattern of Sn–0.7Cu–xIn solder alloys

4.2.2 Immersion Test

The rate of corrosion of Sn-0.7Cu-xIn alloys was assessed non-electrochemically using the traditional weight loss/gain approach. This method is used to calculate the loss of a metal due to corrosion by exposing a metal specimen of a specified area to a corrosive environment for a given time interval and calculating the weight difference before and after exposure. The most often used method of describing corrosion rate is millimeters per year (mm/yr). The formula is used to calculate the rate of corrosion.

$$CPR = \frac{KW}{\rho A t}$$

Where K = constant and a value of 87.6 is taken as a present case.

W = Weight loss in grams

ρ = density of specimen in grams per cubic centimetre

A = expose area in a square centimetre

t = exposure time in an hour

The weight loss experiment of Sn-0.7Cu-xIn samples immersed in 3.5wt. % NaCl lasted 24 weeks, and the results are presented in Fig. 4.3.

Up to 20 weeks, all of the samples demonstrated ongoing weight decrease. The binary Sn-0.7Cu solder alloy has seen the most weight reduction, whereas the ternary Sn-0.7Cu-xIn alloys experienced the least. A slight weight change can be seen in all of the samples after 8 weeks, which might be attributable to the formation of the oxide layer.

Fig. 4.4 shows cumulative weight loss after 24 weeks of exposure. It shows that 3wt.% In solder alloys show the least $(7.24 \pm 0.0213) \times 10^{-4}$ mm/yr, and binary Sn-0.7Cu alloys show the highest corrosion rate $(9.26 \pm 0.016) \times 10^{-4}$ mm/yr.

Table 4. 1 Weight change of Sn-0.7Cu-xIn alloys after immersion in 3.5wt.% NaCl Solution.

Times (Weeks)	**Weight Loss (mg)**			
	In(x=0)	**In(x=1)**	**In(x=2)**	**In(x=3)**
8	0.455	0.442	0.414	0.406
12	0.486	0.472	0.469	0.441
16	0.545	0.491	0.478	0.472
20	0.571	0.517	0.510	0.486
24	0.585	0.524	0.516	0.511

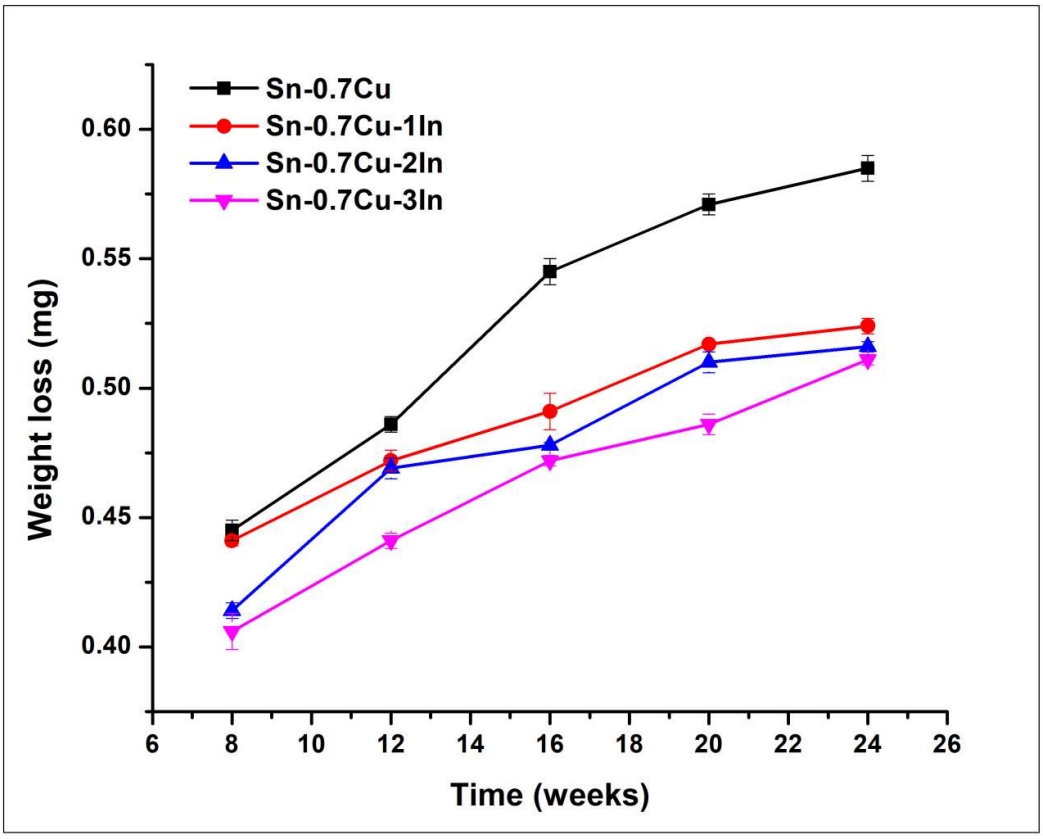

Fig.4. 3 Weight change of Sn-0.7Cu-xIn alloys after immersion in 3.5 wt.% NaCl at room temperature

Table 4. 2 Corrosion rate of Sn-0.7Cu-xIn solder alloys immersion in 0.5M NaCl Solution.

S. No.	Samples	Corrosion Rates * 10^{-4} (mm/yr)
1	Sn-0.7Cu	9.26 ± 0.016
2	Sn-0.7Cu-1In	8.20 ± 0.019
3	Sn-0.7Cu-2In	7.78 ± 0.0147
4	Sn-0.7Cu-3In	7.24 ± 0.0213

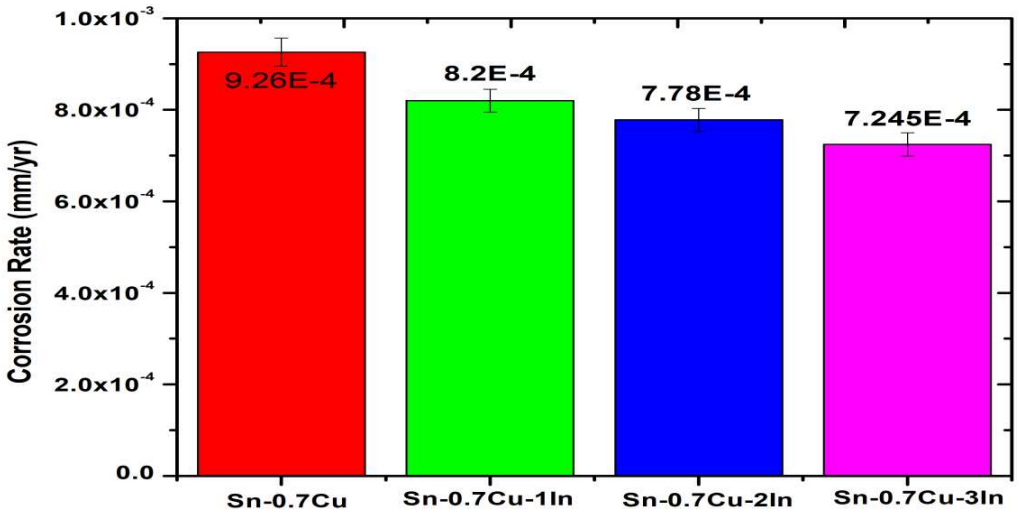

Fig.4. 4 Corrosion rate of Sn-0.7Cu-xIn alloys during static immersion in 3.5 wt.% NaCl at room temperature.

4.2.3 Potentiodynamic Polarization behaviour

Sn-0.7Cu-xIn solder alloys potential current density curve produced by Potential polarization studies done in 3.5%wt aerated NaCl solution in Fig. 4.5; apparently, all the alloys studied exhibit the same polarisation behaviour for variation of Indium form 0 to 3%wt in Sn-0.7Cu-xIn solder alloys. The region of AB in the curve shows the cathodic reaction. During the potentiodynamic polarization experiment, the solution directly reacts with the laboratory atmosphere, the initial oxygen reduction in the neutral and aqueous solution.

$$2H_2O + O_2 + 4e^- \rightarrow 4OH^-_{(aq)} \quad (1)$$

The cathodic reaction was responding to metallic corrosion. It is carried by the oxygen reaction and/or hydrogen reaction. The hydrogen bubble produces at the working (cathode) electrode by the reduction of water molecules and removal of hydrogen ions, which many researchers have reported [144][145][56].

$$2H^{+}_{(aq)} + 2e^{-} \rightarrow H_{2(g)} \quad (2)$$

$$2H_2O + 2e^{-} \rightarrow H_{2(g)} + 2OH^{-}_{(aq)} \quad (3)$$

An anodic reaction in the potentiodynamic polarization tests also occurs in particular regions named BC, CD, DE, and EF, as shown in a curve.

The current density increases dramatically from point B to point C in the anodic region, and corrosion product formation during the experiment has been tracked. It's far typically interpreted that the passivation film formation starts with the precipitation of Sn $(OH)_2$ at the surface. Such corrosion products cover the alloys' surface and protect the substratum alloys against further corrosion; thus, a plateau area (CD) occurs in curves where the current density maintains a relatively stable value of about -4A/cm^2. This stage illustrates Sn's passivation behaviour and subsequent successful dissolution, as shown in Equation 4.

$$Sn + 2OH^{-} \rightarrow Sn(OH)_2 + 2e^{-} \quad (4)$$

A sharp increase in current density is again located when the potential reaches point D, signalling the passivation film's breakdown, usually due to the oxygen evolution reaction in Eq. 4 and the absorption of Cl^{-} by corrosion products. Tin monoxide (SnO) has been considered a semiconductor oxide and may weaken the corrosion resistance. Hence it is detrimental to the passivation film's stability. These results in a sharp peak corresponding to active Sn dissolution induced by Cl^{-} ions with the formation of $SnCl_3^{-}$ and $SnCl_6^{2-}$soluble complexes result in initial pitting, which inevitably breaks the passivation layer consistency. The tin oxide was formed and found to be thermodynamically stable. Therefore so, tin hydroxides can quickly dehydrate to form SnO_2 and SnO.

$$Sn + 2OH^{-} \rightarrow SnO + H_2O + 2e^{-} \quad (5)$$

$$2Sn + O_2 + 2H_2O \rightarrow 2Sn(OH)_2 \quad (6)$$

$$Sn(OH)_2 + 2OH^{-} \rightarrow Sn(OH)_4 + 2e^{-} \quad (7)$$

$$2Sn^{2+} + 6H_2O + O_2 \rightarrow 2Sn(OH)_4 + 4H^+ \quad (8)$$

$$Sn(OH)_4 \rightarrow SnO_2 + H_2O \quad (9)$$

$$3Sn + 4OH^- + 2Cl^- \rightarrow Sn_3O(OH)_2Cl_2 + H_2O + 6e^- \quad (10)$$

Table 4.3 summarizes the relevant Tafel fitting findings of the polarization test. Due to the lack of a well-defined investigation anodic, the corrosion current density (i_{corr}) was determined by extrapolating the cathodic Tafel area. The corrosion potential (E_{corr}) favorably shifted to a more negative value from -770.16 to -731.27 mV, increasing the weight percentage of indium from 1wt.% to 3wt%. The potential corrosion increases with the increases in the indium content of the alloys. A nobler E_{corr} value means that the alloys are thermodynamically resistant to corrosion. Therefore, it is simple to find that adding one weight percentage of In will effectively increase the alloy's corrosion resistance from the thermodynamic aspect. It is also observed that corrosion current density (I_{corr}) value for Sn-0.7Cu solder alloy decreases significantly with the addition of In, especially for Sn-0.7Cu-3In alloys. In general, i_{corr} is a crucial parameter for evaluating the corrosion rate and the kinetics of corrosion reactions at E_{corr}.

As shown in Table 4.3, the addition of Indium in Sn-0.7Cu alloy decreases the I_{corr} value and an improved protective layer of a passivation film on the surface of a sample by including indium. This result may be attributed to the Indium involvement in passivation behaviour, as submitted by Tao- Chil Chang et al. The additional small quantity of Indium in Sn-0.7Cu alloys may increase corrosion resistance. The addition of more indium could possibly give the better corrosion resistance of the above alloys.

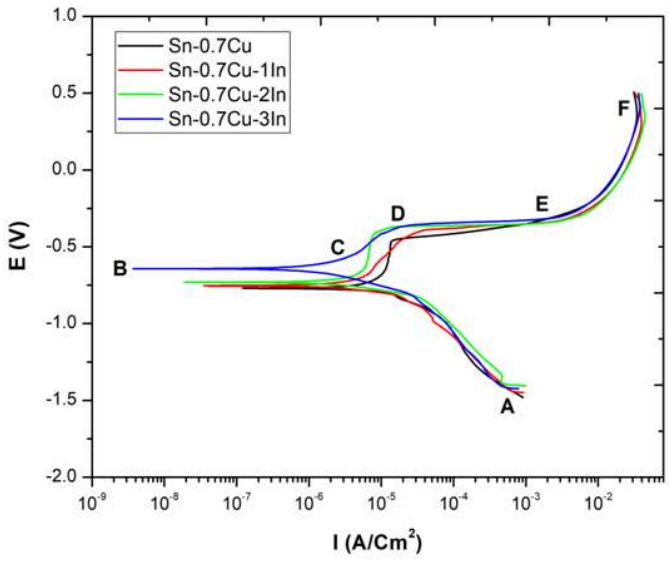

Fig.4. 5 Potentiodynamic polarization curves of Sn–0.7Cu–xIn solder alloys in 3.5wt.% NaCl solution.

Table 4. 3 Polarization parameters for Sn-0.7Cu-xIn alloys in 0.5M NaCl solution

Sample	i_{corr} (μ Amps/cm^2)	E_{corr} (mVolts)	Corrosion Rate (mm/y)* 10^{-2}
Sn-0.7Cu	24.828	-770.16	8.113
Sn-0.7Cu-1In	12.034	-731.27	3.9326
Sn-0.7Cu-2In	4.691	-722.97	1.533
Sn-0.7Cu-3In	2.468	-642.85	0.80654

4.2.3 Electrochemical impedance spectroscopy Analysis

EIS has been used to analyze the corrosion resistance of lead-free solder alloys at OCP. Nyquist plots (complex impedance) and Bode plots for Sn-0.7Cu-xIn (x=0,1,2,3) are illustrated in Fig. 4.6 (a) and 4.6(b). Impedance plots are shown for the different compositions with the variation of indium in solder alloys. It is seen that the Nyquist plots consist of a single depressed semicircle, while the Bode plots indicate a constant presence within the impedance spectra. Current distribution patterns were calculated using electrochemical impedance spectroscopy. If phase angles are greater than 45° in the phase

angle vs. logf plots, the current distribution is uniform in the given frequency region. Therefore an effective corrosion rate can be measured from the potential polarization curve. All indium containing Sn-0.7Cu alloys have a straight line at the low-frequency region, whereas Sn-0.7Cu alloy has a semicircular arc when superimposing with two axes angle of about 45^0. It shows that the corrosion kinetics process shifts from charge transfer control in Sn-0.7Cu alloy to diffusion control in indium-based alloys, known as Warburg impedance. Its means addition of Indium in Sn-0.7Cu alloys changes the corrosion mechanism of alloys. Bode plots are shown in Fig. 4.6(b); most phase angle curves are lower than 90°, which means an ideal capacitance deviation concerning the electrochemical interface is present. In the high-frequency region, the arc radius for Sn-0.7Cu-3In is high compared to the lower composition of indium alloys, which means that Sn-0.7Cu-3In has been the best corrosion-resistant alloy in this study. Two equivalent electrical circuits (EEC) models are used to fit EIS data to Sn-0.7Cu and Indium containing Sn-0.7Cu alloys based on the interpretation above.

Fig. 4.7 shows, A simple equivalent circuit (EC) is reliable to be a Randle cell circuit Rs is the resistance o the solution, CPE_1 and R_1 were related to the capacitance and resistance of the porous product layer of corrosion; CPE_2 and R_2 were related to the capacitance and resistance of the electrical double layer between the alloys interface and the product of corrosion and W related to the Warburg impedance respectively.

The fitting parameter from EIS data ware well-fitting in EEC modal is summarized in table 4.4. The results obtained after fitting are evaluated with a standard deviation (χ^2) at a magnitude of about 10^{-4}. So we may assume that the proposed EEC models are adequate for quantitatively evaluating the electrochemical interface's behaviour.

It should be noted that almost all of the alloys in this experiment contain the same resistance solution (R_s) using the same concentration solution. The R_1 value of such indium-based alloys is often higher than that of the Sn-0.7Cu alloy R_1 reflects corrosion resistance of a porous surface layer of corrosion, as described above, and it can be concluded that the introduction of indium will lead to a more protective surface layer of corrosion. To quantitatively evaluate the total corrosion resistance to corrosion of the solder alloys introduced by $R_t = R_w+R_1+R_2$ [146][147]. Throughout this study, the total resistance of alloys extended due to the Warburg impedance in this experiment; solution resistance R_S is not considered because it is almost constant due to the same solution. Therefore total Resistance of Sn-0.7Cu-xIn (x=0, 1, 2, 3) is 0.2236, 4.9145, 10.1635 and 22.4202 kΩ respectively. It is seen that R_1 increases with the increase in Indium content Indium in alloys. Therefore then, Sn-0.7Cu-3In has the highest Rt value. It can be inferred from the observation that the indium addition in the Sn-0.7Cu alloy will improve the corrosion resistance in this experiment.

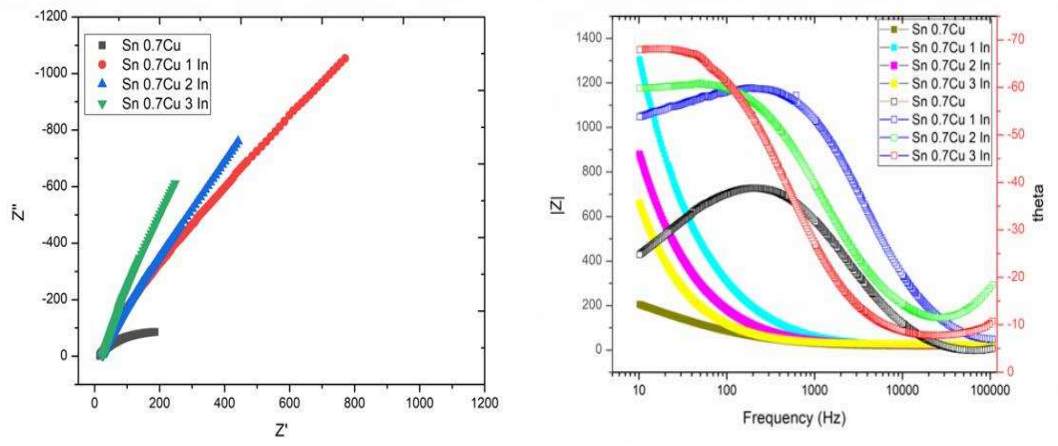

Fig.4. 6 (a) Nyquist and (b) Bode plots of solder alloys in 0.5M NaCl solution.

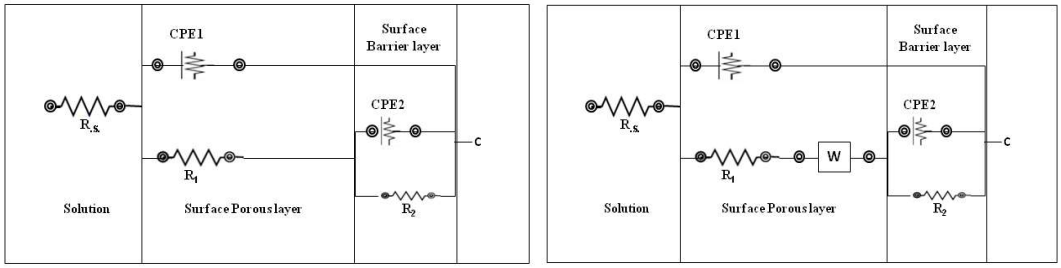

Fig.4. 7 Electrical circuit models. (a) For Sn-0.7Cu alloy; (b) For Sn-0.7Cu alloys with Indium addition

Table 4. 4 Fitting parameters of EEC for Sn-0.7Cu-xIn alloys in 0.5M NaCl solution

Sample	R_s	R_1	CPE_1		R_2	CPE_2		R_w	χ^2 *
	Ωcm^2	Ωcm^2	Y_1*10^{-6} $\Omega cm^{-2}s^n$	n_1	Ωcm^2	Y_2*10^{-6} $\Omega cm^{-2}s^n$	n_2	Ωcm^2	10^{-4}
Sn-0.7Cu	14.54	21.19	127.86	0.69	202.5	178.71	0.62		0.15477
Sn-0.7Cu-1In	18.7	7.556	26.92	0.75	1807	29.849	0.71	3100	0.1611
Sn-0.7Cu-2In	17.14	21.55	450.59	0.49	5476	45.482	0.75	4666	1.8286
Sn-0.7Cu-3In	19.1	25.75	376.02	0.58	22393	51.733	0.58	1.49	1.3499

4.3 Characterization of corrosion products

Surface topography of solder alloys was done by SEM and composition analysis by EDS and XRD. It was done before and after the electrochemical corrosion in 0.5M NaCl. Generally, the morphology of alloys' surfaces changes forms smooth to porous due to the formation of branched crystallites, networked branches, and platelet-like and sponge-like structures. EDS and XRD analysis have recognized such compounds as mainly tin oxide and other corrosion products. The addition of indium from 1 wt% to 3 wt% in binary Sn-0.7Cu solders in Fig. 4.8 shows that all the solder alloys surface after corrosion was covered by a sponge platelet-like structure of different sizes. It has been observed that sponge-like structures are denser in the Sn-0.7Cu-3In sample than in the Sn-0.7Cu solder alloys. There is not much difference in quantity and morphology of corrosion products

Sn-0.7Cu and Sn-0.7Cu-1In. It is expected that the properties of corrosion products on the surface alloys should be denser, more refined, and continuous. Because it improves corrosion resistance by effectively protecting corrosion of alloys, it is evident from the EIS results that RP values for the porous product layer are higher, which is very valid for the denser porous product layer. Therefore, the denser product layer on the solder alloys is very much helpful for the better corrosion resistance of the Sn-Cu-In alloys.

The EDX analysis of corrosion products of alloys is shown in Fig. 4.10 for all alloys taken for these investigations. There is a quite significant quantity of O, Na, Cl, Cu, and Sn present on the surface of the alloys after corrosion, while the Indium weight percentage is significantly less. The atomic percentage of Sn, H, Cl, and O in the corrosion products is more likely to consist of $Sn_3O(OH)_2Cl_2$ on alloys' surfaces as a dominant product, mostly combined with small quantities of oxide compounds.

The XRD analysis was further carried out to confirm the phase composition of the corrosion products. Chloride can be explained by the presence of by-products of corrosion like chloride can be explained by the presence of by-products of corrosion like $Sn_3O(OH)_2Cl_2$ [148] and $Sn_4(OH)_6Cl_2$ [101] on the surface of alloys, and shown in Fig. 4.11.

First, during the corrosion process, the surface layer decomposition and then pitting corrosion generally occur [149][150]. Different kinds of models have been suggested to explain the corrosion mechanism in which aggressive anions such as OH^- and Cl^- play a significant role. It has been observed that faceted IMC of Cu_6Sn_5/Cu_3Sn and non-faceted β-Sn phase [151] are present in these lead-free solder alloys. Cu_6Sn_5/Cu_3Sn particles are electrochemically nobler than tin. Therefore, a galvanic cell may be formed between the

Sn-rich phase and IMC Cu_6Sn_5/Cu_3Sn, accelerating Sn-0.7Cu-xIn alloy's anodic corrosion.

Furthermore, the microstructural arrangement sets different cathode/anode area ratios. This is closely linked to the morphology and uniform distribution, as well as to the network interconnectivity level in the (noble) stage of the cathode (dendritic) cellular arrays [58]. For example, an integrated, interconnected network of IMC Cu_6Sn_5 formed in Sn-0.7Cu solder alloy [57] changes the cathode-anode ratio significantly with corrosion action. This increases the cathode area formed by Cu_6Sn_5 IMC, whereas the sn-rich matrix is corroded intensely and more rapidly. The IMC of Cu_6Sn_5/Cu_3Sn thickness ratio decreases due to adding Indium particle in binary Sn-0.7Cu solder alloy, improving corrosion resistance [152].

The cathodic reaction results in the formation of OH^- ions. Sn dissolution starts with an anodic reaction which results in the formation of $Sn(OH)_2^-$ Generally, Sn^{n+} has a valance state of n=2 and n=4, and it undergoes in scale form of Sn^{2+} or Sn^{4+} by giving e^{2-} or e^{4-}. The diffusion of Sn^{2+} atoms along the grain boundary results in the formation of a vacancy in the fat matrix. The reaction between these ions results in the formation of uniform $Sn(OH)_2$ and $Sn(OH)_4$ films, and the dehydration reaction of $Sn(OH)_2$ leads to the formation of SnO at the surface. The diffusion of Sn from the SnO layer at the surface results in the formation of vacancies in the oxide layer. The dissolution of the oxide layer starts with the transfer of Sn ions from the SnO layer to the electrolyte, which results in the formation of $Sn(OH)_2$ in the electrolyte. This results in localized thinning of the film. The diffusion of Sn ions from the oxide layer causes the generation of vacancies in SnO film more quickly at the scale matrix interface, resulting in a breakdown of the passive SnO layer. Cl^- anion attacks on the Sn matrix result in pits forming at the surface, as shown in Fig. 4.8 and 4.11.

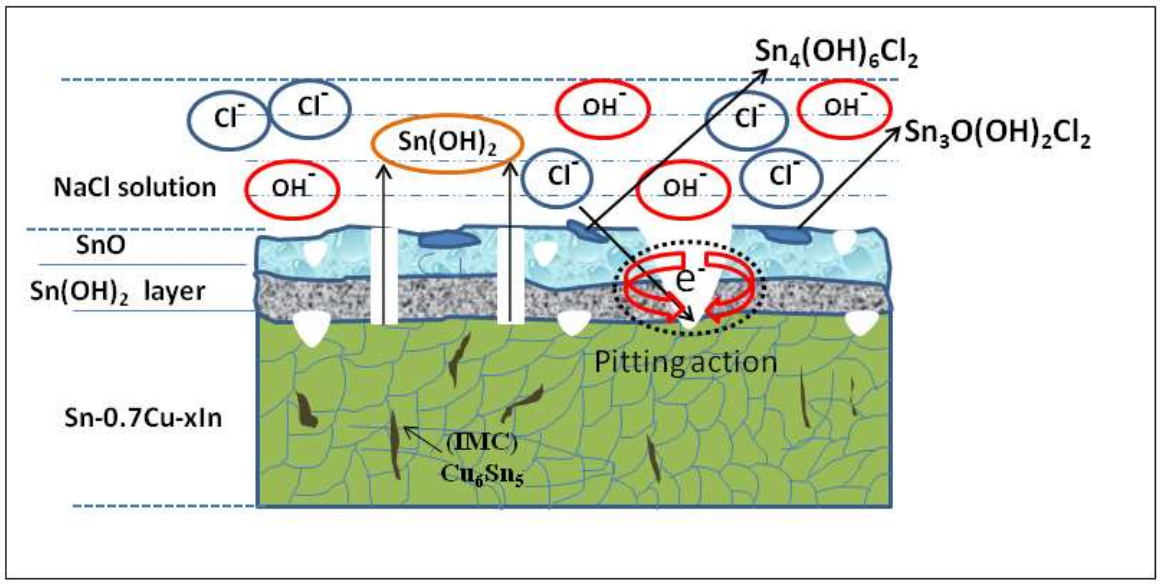

Fig.4. 8 Corrosion Mechanism of Solder alloys

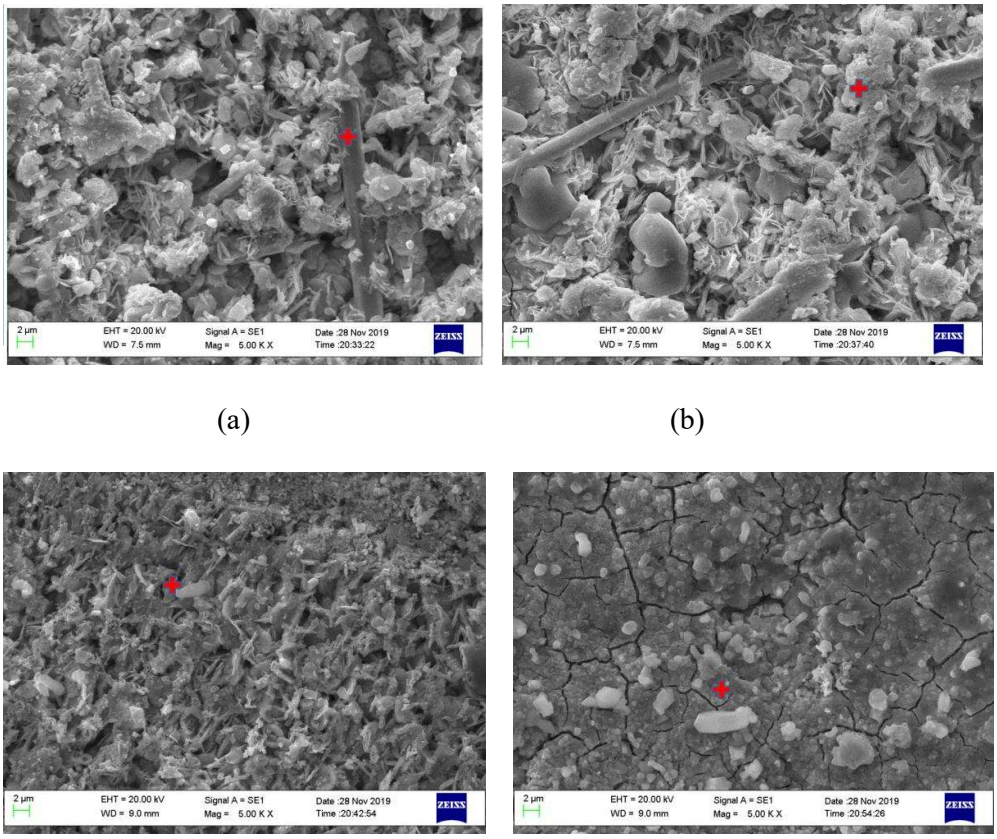

(a) (b)

(c) (d)

Fig.4. 9 Surface morphology of alloys after corrosion in 3.5wt.% NaCl. (a) Sn- 0.7Cu; (b) Sn-0.7Cu-1In; (c) Sn-0.7Cu-2In; (d) Sn-0.7Cu-3In

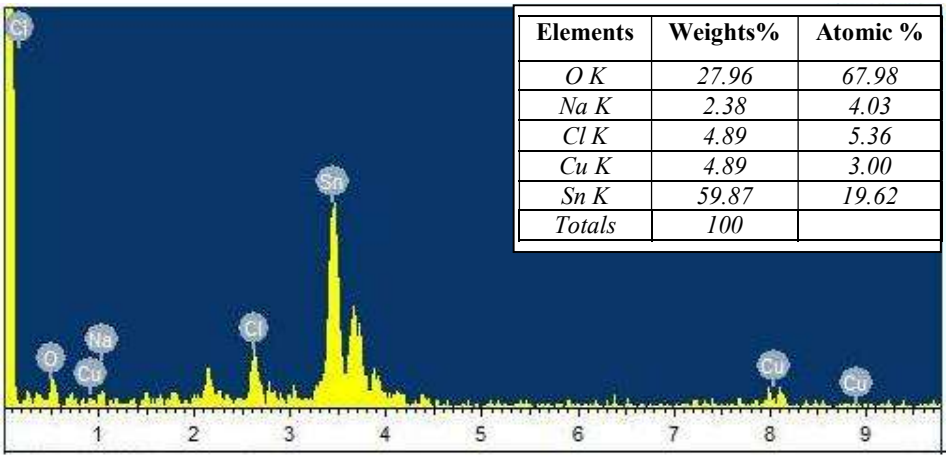

Elements	Weights%	Atomic %
O K	*27.96*	*67.98*
Na K	*2.38*	*4.03*
Cl K	*4.89*	*5.36*
Cu K	*4.89*	*3.00*
Sn K	*59.87*	*19.62*
Totals	*100*	

(a)

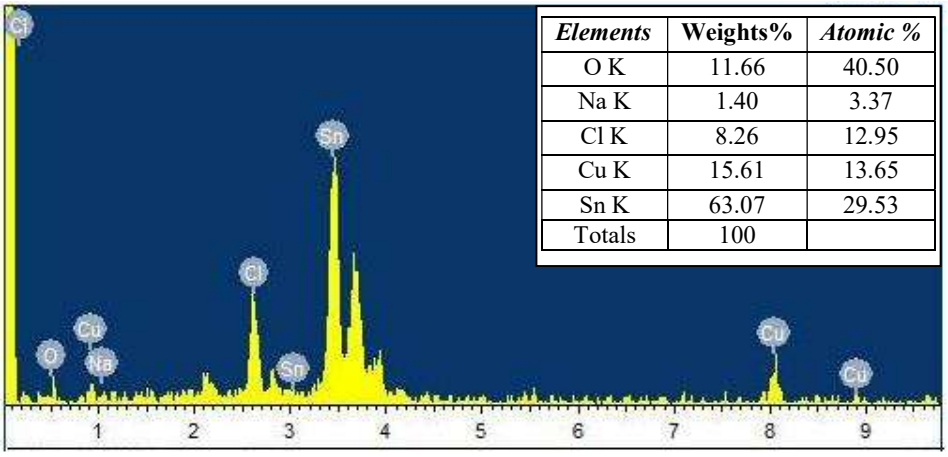

Elements	Weights%	*Atomic %*
O K	11.66	40.50
Na K	1.40	3.37
Cl K	8.26	12.95
Cu K	15.61	13.65
Sn K	63.07	29.53
Totals	100	

(b)

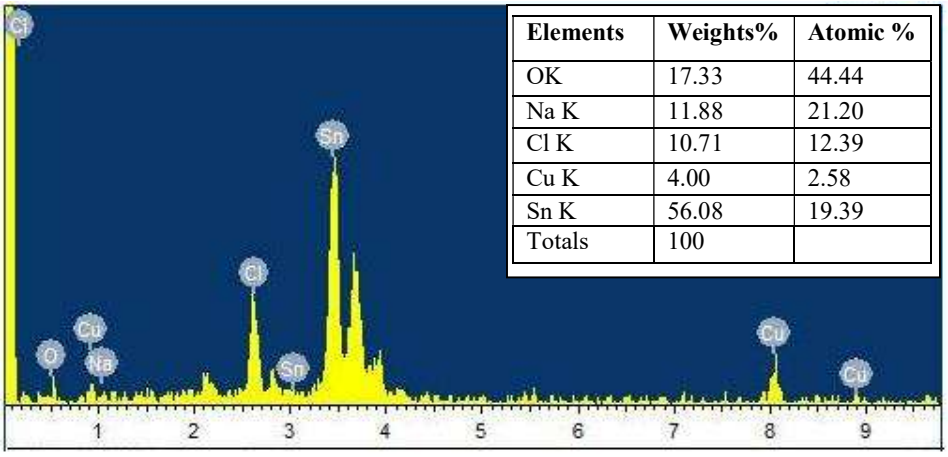

Elements	Weights%	Atomic %
OK	17.33	44.44
Na K	11.88	21.20
Cl K	10.71	12.39
Cu K	4.00	2.58
Sn K	56.08	19.39
Totals	100	

(c)

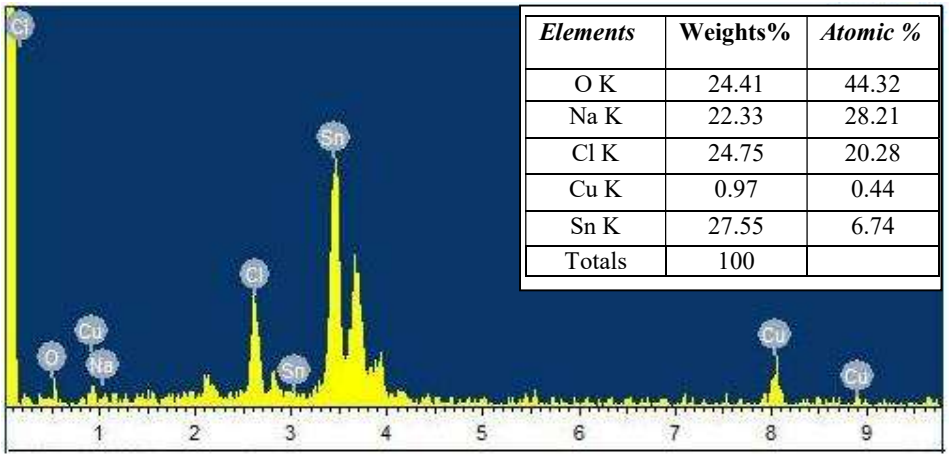

Elements	Weights%	*Atomic %*
O K	24.41	44.32
Na K	22.33	28.21
Cl K	24.75	20.28
Cu K	0.97	0.44
Sn K	27.55	6.74
Totals	100	

(d)

Fig.4. 10 EDX patterns of corrosion products. (a) Sn-0.7Cu; (b) Sn-0.7Cu-In; (c) Sn-0.7Cu-2In; (d) Sn-0.7Cu-3In.

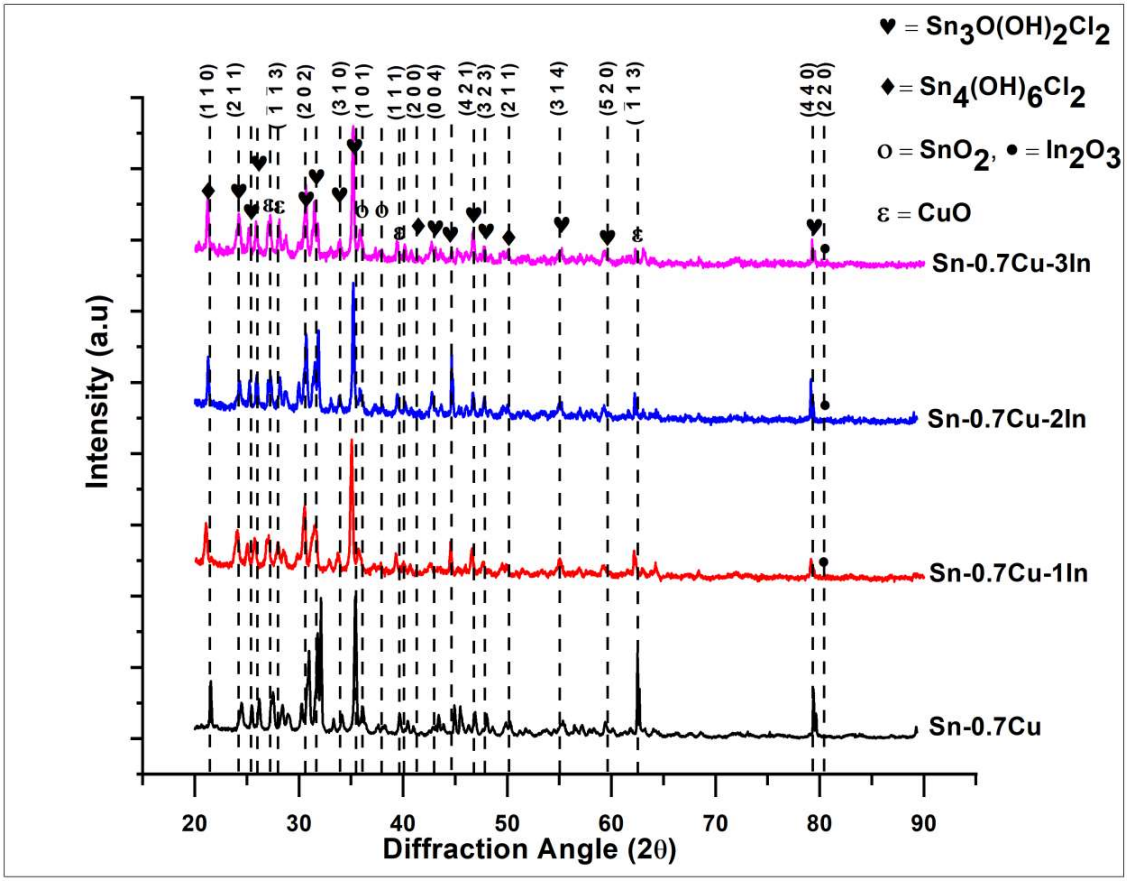

Fig.4. 11 XRD patterns of corrosion products. (a) Sn-0.7Cu; (b) Sn-0.7Cu-1In; (c) Sn-0.7Cu-2In; (d) Sn-0.7Cu-3In.

4.4 Conclusions

The electrochemical behaviour of Sn-0.7Cu-xIn lead-free solder alloys in a natural 3.5 wt % NaCl was studied by potentiodynamic polarization tests and EIS measurements. The impact of Indium content on corrosion properties of Sn-0.7Cu-xIn solder alloys was investigated, and the following conclusions were drawn from these studies.

- An increase of indium content from 1 to 3 weight percentage leads to a significant improvement in corrosion resistance of Sn-0.7Cu solder alloys, resulting in a higher range of pseudo passivation and lower current density pseudo passivation.
- The addition of Indium to Sn-Cu binary solder alloys β-Sn grains have significantly. The resulting microstructure of refined solder alloys now has a more uniform distribution of various phases, which is responsible for improving corrosion resistance.
- The addition of Indium in Sn-0.7Cu solder alloys modifies the morphology of corrosion products on alloys' surfaces and changes the corrosion kinetics from the charge transfer to the diffusion control process.
- The corrosion products on the surface of all solder alloys studied after potentiodynamic polarisation consists of tin oxide chloride hydroxide $Sn_3O(OH)_2Cl_2$ and $Sn_4(OH)_6Cl_2$. Most corrosion products have plate-like shapes and are loosely distributed on the surface with different orientations.